Scattering of surface plasmons on graphene by a discontinuity in surface conductivity

2015 J. Opt. 17 075002

(http://iopscience.iop.org/2040-8986/17/7/075002)

IOP Publishing Journal of Optics
J. Opt. 17 (2015) 075002 (8pp) doi:10.1088/2040-8978/17/7/075002

Scattering of surface plasmons on graphene by a discontinuity in surface conductivity

Behzad Rejaei and Amin Khavasi

Department of Electrical Engineering, Sharif University of Technology, PO Box 11155-4363, Tehran, Iran

E-mail: khavasi@sharif.edu

Received 18 February 2015, revised 26 April 2015
Accepted for publication 29 April 2015
Published 10 June 2015

Abstract

The scattering of graphene surface plasmons from an arbitrary, one-dimensional discontinuity in graphene surface conductivity is treated analytically by an exact solution of the quasi-static integral equation for surface current density in the spectral domain. It is found that the reflection and transmission coefficients are not governed by the Fresnel formulas obtained by means of the effective medium approach. Furthermore, the reflection coefficient generally exhibits an anomalous reflection phase, which has so far only been reported for the particular case of reflection from abrupt edges. This anomalous phase becomes frequency-independent in the regime where the effect of inter-band transitions on graphene conductivity is negligible. The results are in excellent agreement with full-wave electromagnetic simulations, and can serve as a basis for the analysis of inhomogeneous graphene layers with a piecewise-constant conductivity profile.

Keywords: graphene, surface plasmons, scattering

1. Introduction

Surface plasmons on graphene, a mono-atomically thick layer of carbon [1], have recently attracted much attention due to their strong spatial confinement and long lifetimes. Graphene plasmons (GPs), which propagate on doped or gated layers, are essentially electromagnetic surface waves bound to waves of surface charge density [2]. Because of their short wavelengths, they are promising candidates for the realization of miniaturized THz and optical devices such as absorbers [3], waveguides [4], optical circuit elements [5], and antennas [6].

An attractive feature of GPs is the tunability of their properties by local modulation of surface conductivity. This feature forms the basis of graphene-based transformation optics [7] and tunable planar lenses [8, 9]. Yet, the analysis of such devices requires a thorough understanding of the effect of variations in surface conductivity on the propagation of GPs.

Although the scattering of GPs in some special cases, e.g., line defects [10] and abrupt edges [11], have been studied, less is known about their scattering from an arbitrary, one-dimensional (1D) discontinuity in surface conductivity. Once computed, the scattering parameters of a discontinuity can be used in scattering or transfer matrix calculations to analyze inhomogeneous graphene layers with piecewise-constant, but otherwise arbitrary, conductivity profiles. For such structures, many authors currently use a simple model for GP scattering in which each part of the graphene layer is modeled by an effective medium characterized by the complex effective index of the propagating GP mode [7–9, 12]. Based on this assumption, whose relative success is numerically demonstrated, reflection and transmission from a discontinuity can be obtained [12].

In this paper, we present an analytical calculation of the scattering parameters of GPs normally incident on a 1D discontinuity in graphene surface conductivity. By analytically solving the quasi-static integro-differential equation for surface current density in the spectral domain, closed-form results are found for the reflection and transmission coefficients. The presented analysis is rigorous, and the results are in excellent agreement with full-wave electromagnetic simulations as long as the quasi-static approximation is valid. Our analytical calculations show that the reflected and transmitted power from a discontinuity are correctly predicted by the aforementioned effective medium model. However, the reflection and transmission coefficients themselves are not governed by the Fresnel formulas obtained by means of the effective medium approach.

Moreover, the reflection coefficient generally exhibits an anomalous reflection phase that had so far only been reported for the particular case of reflection from abrupt edges [11]. This anomalous phase, which is due to the evanescent fields generated near the discontinuity, becomes frequency-independent in the regime where the effect of inter-band transitions on graphene conductivity is negligible.

2. Scattering of GPs by an abrupt change in surface conductivity

The electromagnetic properties of graphene are described by a frequency-dependent surface conductivity σ_s which, within the random-phase approximation [13], is given by

$$\sigma_s = \frac{e^2 E_F}{\pi\hbar^2}\frac{1}{\tau^{-1} - i\omega} + \frac{e^2}{4\hbar}\left[H\left(\hbar\omega - 2E_F\right) + \frac{i}{\pi}\ln\left|\frac{\hbar\omega - 2E_F}{\hbar\omega + 2E_F}\right|\right]. \quad (1)$$

Here e is the electron charge, E_F is the Fermi energy, $\hbar$ is the Plank constant, H is the Heaviside step function, τ is the relaxation time, and ω is the radial frequency (a time dependence of $e^{-i\omega t}$ will be assumed throughout this paper). Strictly speaking, equation (1) is only valid when $E_F \gg k_B T$ and $\left|E_F - \hbar\omega/2\right| \gg k_B T$ where k_B is the Boltzmann constant and T is the temperature. A more general expression for σ_s can be found in [14].

At frequencies where $\tau^{-1} \ll \omega < 2E_F/\hbar$, σ_s is predominantly a positive imaginary quantity. The graphene sheet thus exhibits an inductive surface impedance, which, in combination with the electromagnetic interaction between its charge carriers through the surrounding environment, leads to the propagation of GPs. The wavelength of GPs depends on σ_s and, therefore, the Fermi energy. Local variation of E_F, e.g., by doping or applying a gate potential, results in a position-dependent surface conductivity, which affects the GP propagation.

In order to study the propagation and reflection of GPs in the presence of inhomogeneities in σ_s, consider a sheet of graphene covering the $x-y$ plane and surrounded by dielectric half-spaces with the permittivities ϵ_0 ($z > 0$) and ϵ_1 ($z < 0$) as in figure 1. It is assumed that the graphene layer is described by a position-dependent surface conductivity $\sigma_s(x)$. Moreover, for later purposes, we initially assume the presence of external sources, which are uniform in the y-direction and, in the absence of the graphene layer, produce a p-polarized electric field $\boldsymbol{E} = E_x^{ex}\hat{\boldsymbol{x}} + E_z^{ex}\hat{\boldsymbol{z}}$. Within the quasi-static approximation [5], the equation governing the behavior of the induced surface current $\boldsymbol{J}_s = J_x(x)\hat{\boldsymbol{x}}$ is [15]

$$\frac{J_x(x)}{\sigma_s(x)} = E_x^{ex}(x) + \frac{1}{2\pi i\omega\epsilon_e}\int_{-\infty}^{\infty}\frac{1}{x-x'}\frac{dJ_x(x')}{dx'}dx', \quad (2)$$

where $\epsilon_e = (\epsilon_0 + \epsilon_1)/2$. The integral is of the Cauchy principal-value type. Equation (2) simply states that at any point on the graphene surface, J_x equals σ_s times the total electric field, which consists of the external field E_x^{ex} and the field due to the surface charge density $\rho_s = (i\omega)^{-1}dJ_x/dx$ (the second term on the right hand side of (2)).

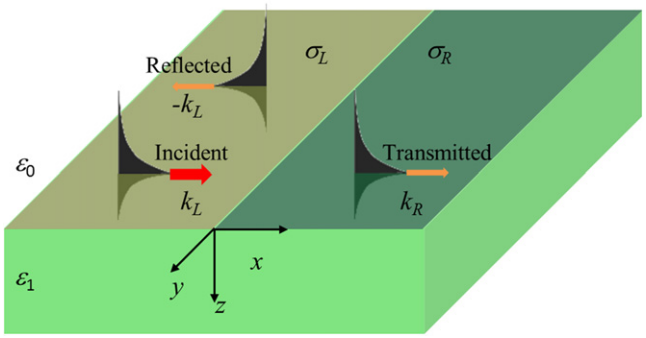

Figure 1. A graphene layer surrounded by two semi-infinite media with the dielectric constants ϵ_0 and ϵ_1. The graphene surface conductivity is σ_L and σ_R for $x < 0$ and $x > 0$, respectively. A plasmonic wave traveling with the wavenumber k_L in the region $x < 0$ is scattered by the discontinuity at $x = 0$.

Before using (2) to treat the scattering of GPs from a discontinuity in σ_s, it is instructive to investigate its solution for a uniform graphene layer with a constant surface conductivity $\sigma_s(x) = \sigma_0$. After applying a Fourier transform to (2), and using the relationship

$$\frac{1}{\pi} - \int_{-\infty}^{\infty}\frac{e^{-ikx}}{x-x'}dx = -i\ \mathrm{sgn}(k)e^{-ikx'}, \quad (3)$$

one finds the Fourier transform of the surface current density induced by the external sources on a uniform layer to be given by

$$\tilde{J}_{x,0}(k) = \int_{-\infty}^{\infty} J_{x,0}(x)e^{-ikx}dx = \frac{2i\omega\epsilon_e}{k_P - |k|}\int_{-\infty}^{\infty} E_x^{ex}(x)e^{-ikx}dx, \quad (4)$$

where $k_P = 2i\omega\epsilon_e/\sigma_0$. The latter quantity is, in fact, the propagation constant of the plasmonic wave in the quasi-static approximation: the solution given by (4) has a pole at $k = \pm k_P$ which implies that in the absence of sources, waves propagating with the wave number k_P are the natural solutions of the system.

Let us next return to equation (2) and focus on a graphene layer where $\sigma_s(x)$ undergoes an abrupt change at $x = 0$ due to an abrupt transition in Fermi energy. We shall denote the surface conductivity on the two sides of the junction by $\sigma_s(x) = \sigma_L, \sigma_R$ for $x < 0$ and $x > 0$, respectively (figure 1). The local values of the GP propagation constant are

$$k_L = \frac{2i\omega\epsilon_e}{\sigma_L},\ k_R = \frac{2i\omega\epsilon_e}{\sigma_R} \quad (5)$$

in these regions.

Due to the position dependence of σ_s, application of a Fourier transform to (2) does not directly yield the solution as in the case of a uniform graphene sheet. Therefore, one has to resort to a more elaborate mathematical technique whose details are presented in appendix A. It turns out that despite the non-uniformity of σ_s, equation (2) can still be solved

analytically in the spectral domain for the conductivity profile defined earlier. The results obtained are then used to analyze the scattering of a current density wave

$$J_x^i(x) = Ae^{ik_L x}, \tag{6}$$

that is produced by external sources in the region $x < 0$ and is incident on the junction at $x = 0$ from the left (see appendix C for the full description of the electromagnetic field accompanying a GP). It is shown that well away from the discontinuity at $x = 0$, the scattered current density is given by the reflected and transmitted waves

$$J_x^r(x) = rAe^{-ik_L x},\ J_x^t(x) = tAe^{ik_R x}, \tag{7}$$

for $x < 0$ and $x > 0$, where

$$r = e^{i\vartheta}\frac{k_L - k_R}{k_L + k_R},\ t = \frac{2(k_L k_R)^{1/2}}{k_L + k_R}, \tag{8}$$

are the coefficients of reflection and transmission, respectively. The phase ϑ is given by

$$\vartheta = \frac{\pi}{4} - \frac{2}{\pi}\int_0^\infty \frac{\arctan\left(k_L u/k_R\right)}{u^2 + 1}du. \tag{9}$$

The scattering parameters for a wave with the wave number k_R, incident on the junction from the right, can simply be found by exchanging k_L and k_R in (8). Using (9), it can be shown that ϑ would then acquire a minus sign. Note also that, under quasi-static approximation, the reflected and transmitted powers of GP are $|r|^2$ and $|t|^2$, respectively, as shown in appendix C.

It is worth mentioning that the reflection and transmission coefficients obtained from the effective medium model by using Fresnel equations are:

$$r_{\text{Fresnel}} = \frac{k_L - k_R}{k_L + k_R},\ t_{\text{Fresnel}} = \frac{2k_L}{k_L + k_R}. \tag{10}$$

Obviously, the transmission amplitude and the reflection phase in this equation are different from those derived in (8). Take notice, however, that the results of the effective medium model for the reflected and transmitted powers, respectively, $|r_{Fresnel}|^2$ and $|t_{Fresnel}|^2 k_R/k_L$ [12], are exactly the same as those obtained in this work, namely $|r|^2$ and $|t|^2$, respectively.

It is important to bear in mind that (7) equals the scattered field only sufficiently far away from the discontinuity. The exact expression for the scattered field is given by the inverse Fourier transform of (A.17), (A.20) in appendix A and contains evanescent fields that decay rapidly away from the junction at $x = 0$. Mathematically speaking, the reflected and transmitted waves in (7) correspond to the poles of (A.17), (A.20), whereas the evanescent fields are related to their branch cuts. These evanescent modes are generally responsible for the anomalous reflection phase ϑ in (8) [11].

It is particularly interesting to examine the limit $\sigma_R \to 0$ ($E_{F,R} \to 0$, $k_R \to \infty$), which corresponds to the situation where the graphene sheet on the right side of the junction vanishes and the plasmonic waves on the left side are reflected by an abrupt edge. While the magnitude of r will then equal unity, equation (9) yields $\vartheta = \pi/4$, which results in an overall reflection phase of $-3\pi/4$. The extra phase of $\pi/4$ has been reported in [11] and stems from the excitation of the aforementioned evanescent modes near the edge.

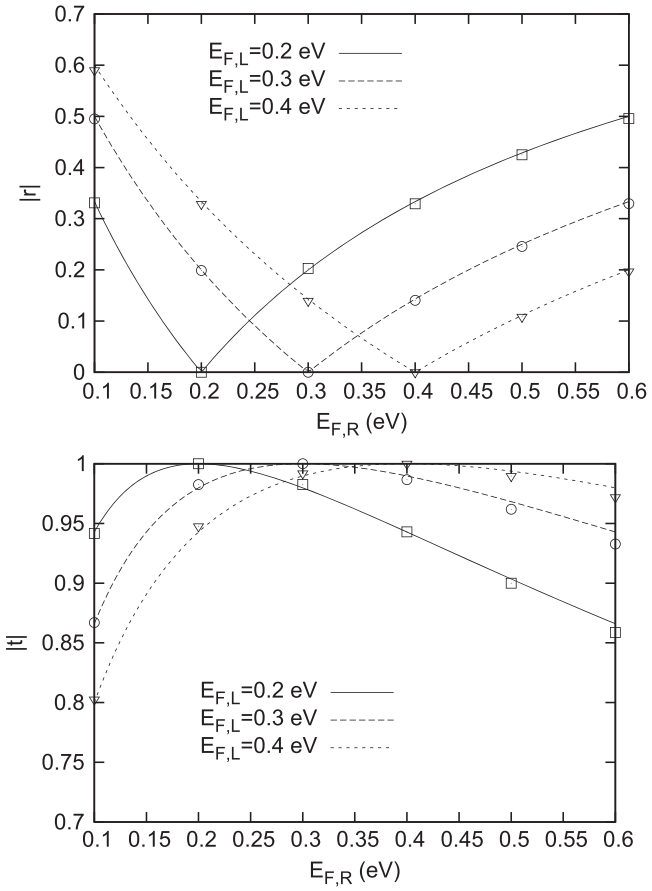

Figure 2. Magnitude of the reflection (top) and transmission (bottom) coefficients of GPs as a function of $E_{F,R}$ for $E_{F,L} = 0.2$, 0.3 and 0.4 eV. The calculations were carried out at 10 THz. Results of full-wave electromagnetic simulations, which were carried out by using corresponding values of σ_R and σ_L, are shown by markers. For these simulations, a relaxation time of $\tau = 5 \times 10^{-12}$ sec was assumed.

3. Discussion of the results

Figures 2 and 3 show the magnitude of r and t and the phase of r as a function of $E_{F,R}$ for several values of $E_{F,L}$ at a frequency of 10 THz. In order to validate the results obtained, full-wave simulations were also performed using Ansoft's high frequency structure simulator (HFSS) for a free-standing graphene layer in a vacuum. Excellent agreement can be observed. The error in the transmission coefficient increases slightly for higher values of Fermi energies, which is caused by the reduced accuracy of the quasi-static approximation as the corresponding plasmonic wavelength becomes comparable to the electromagnetic wavelength in the surrounding environment. The distribution of the x-component of the electric field near the junction is shown in figure 4 for $E_{F,L} = 0.3$ eV and $E_{F,R} = 0.15$, 0.3, 0.6 eV. As mentioned in the previous section, in addition to reflected and

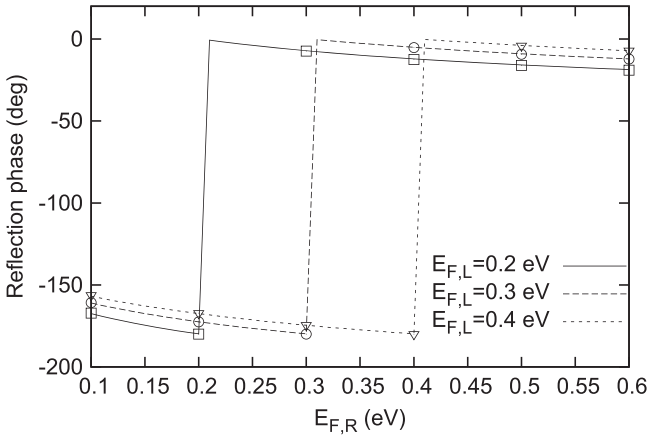

Figure 3. Reflection phase of GPs (dashed line) as a function of $E_{F,R}$ for $E_{F,L} = 0.2$, 0.3 and 0.4 eV. Results of full-wave electromagnetic simulations are shown by markers (circles). The transmission phase is identically zero (not shown).

transmitted waves, the scattered field contains evanescent terms, which are visible near the junction, but decay rapidly as one moves away from $x = 0$.

Equations (8) and (9) show that in the quasi-static approximation, the scattering parameters of GPs that are incident on a discontinuity in surface conductivity only depend on the ratio $k_R/k_L = \sigma_L/\sigma_R$ [see (5)]. In the regime where $\hbar\omega/2 \ll E_{F,L}$, $E_{F,R}$, the second term on the right-hand side of (1), which stems from inter-band transitions in graphene, becomes negligibly small so that $\sigma_L/\sigma_R \approx E_{F,L}/E_{F,R}$. As a result, the reflection and transmission coefficients will only depend on the ratio of the Fermi levels on the two sides of the junction. The reflection phase, as well as the magnitudes of r and t, thus become frequency-independent.

4. Conclusion

We presented analytical results for the scattering parameters of graphene plasmons normally incident on a 1D discontinuity in graphene surface conductivity by exactly solving the quasi-static integro-differential equation for surface current density. The results are in excellent agreement with full-wave electromagnetic simulations. It was found that unlike transmitted and reflected power, the reflection and transmission coefficients are not governed by the Fresnel formulas obtained by means of the effective medium models. Besides, the reflection coefficient generally exhibits an anomalous reflection phase, which is due to the evanescent fields generated near the discontinuity, and becomes frequency-independent in the regime where the effect of inter-band transitions on graphene conductivity is negligible.

The scattering parameters obtained can be used to analyze inhomogeneous graphene layers with 1D (approximately) piecewise-constant surface conductivity profiles by means of conventional scattering or transfer matrix methods. A necessary condition here is that adjacent discontinuities are not too close to each other to avoid the overlap of their evanescent fields. These evanescent fields, which result from the branch-cut integrals in the inverse Fourier transform of (A.17), (A.20), decay rapidly on both sides of a discontinuity, within a fraction of the plasmonic wavelength.

The method outlined can be extended to graphene layers on more complicated, multi-layered substrates, by replacing the kernel of the integral in (2) by the electric-field Green's function of the multi-layered configuration. Equation (2) can also serve as a basis for the treatment of arbitrary (not necessarily stepwise) conductivity profiles. However, since the analytical method outlined in appendix A is only applicable to an abruptly changing surface conductivity, (2) has then to be solved numerically. The same equation can, in principle, be used to investigate the scattering of GPs by inhomogeneities in the substrate dielectric constant, although the corresponding Green's function is rather complicated to compute. Note also that the method outlined in appendix A is well capable of handling complex propagation constants, even though the results presented were obtained by assuming real-valued k_L, k_R. The latter simplification was only made to allow analytical calculation of the integrals involved.

Acknowledgments

The authors would like to thank Dr.A.Borji for many useful discussions.

Appendix A. Exact solution of the current density integral equation for a surface conductivity with a step profile

In this appendix we present the steps required for the derivation of the exact solution of (2) for the structure depicted in figure 1. Let us introduce the one-sided Fourier transforms

$$F_L(\xi) = \int_{-\infty}^{0} J_x(x) e^{-i\xi x} dx, \tag{A.1}$$

$$F_R(\xi) = -\int_{0}^{\infty} J_x(x) e^{-i\xi x} dx, \tag{A.2}$$

in which F_L, F_R are analytical functions of ξ in the upper and lower halves, respectively, of the complex ξ-plane. After applying a Fourier transform to (2), using (3), and rearranging the resulting terms, one obtains

$$F_L(k) = \nu(k) F_R(k) + s(k), \tag{A.3}$$

where $F_L(k)$, $F_R(k)$ are the limiting values of (A.1), (A.2) as the real axis ($\xi = k$) is approached from above and below, respectively, and

$$\nu(k) = \frac{k_R - |k|}{k_L - |k|}, \tag{A.4}$$

$$s(k) = \frac{2i\omega\epsilon_e}{k_L - |k|} \int_{-\infty}^{\infty} E_x^{ex}(x) e^{-ikx} dx, \tag{A.5}$$

where k_L, k_R are given by (5). For later purposes, take notice that $s(k)$ is the Fourier transform of the surface current

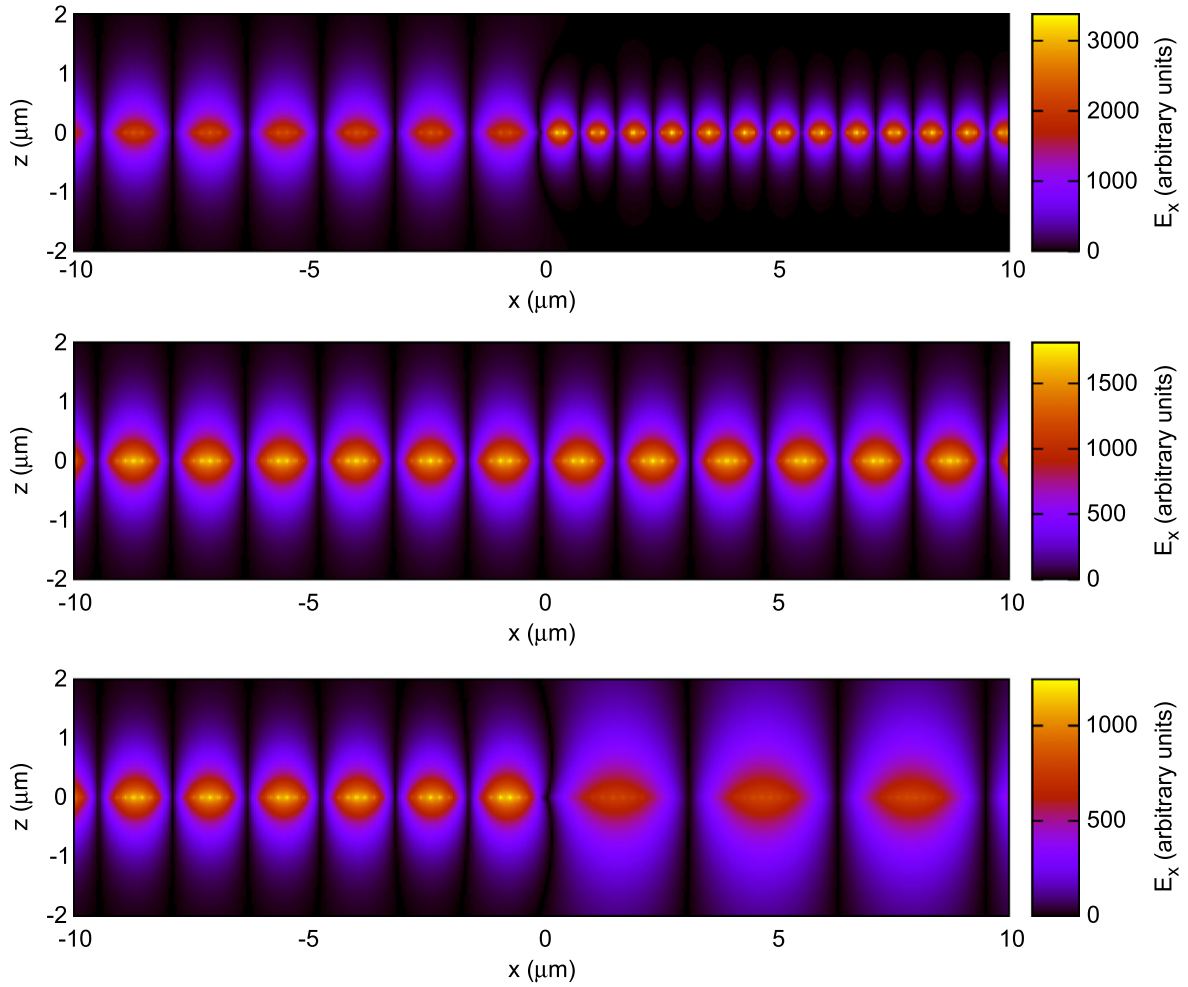

Figure 4. Distribution of the x-component of the electric field (real part) in the vicinity of a free-standing graphene layer for $E_{F,L} = 0.3$ eV and $E_{F,R} = 0.15$ eV (top), $E_{F,R} = 0.3$ eV (middle), and $E_{F,R} = 0.6$ eV (bottom). The incident plasmonic wave travels towards the discontinuity at $x = 0$ from the left. The calculations were carried out at 10 THz.

density,

$$\tilde{J}_x(k) = \int_{-\infty}^{\infty} J_x(x) e^{ikx} dx = F_L(k) - F_R(k), \tag{A.6}$$

that external sources induce on a graphene layer with a uniform surface conductivity σ_L. This can be shown by direct comparison of (A.5) with (4).

The problem has thus been reduced to that of finding the functions $F_L(\xi)$ and $F_R(\xi)$, which are analytical in their respective halves of the complex ξ-plane and satisfy (A.3) on the entire real axis. This is an inhomogeneous Hilbert problem, which is frequently encountered in the solution of singular integral equations [16]. The solution is formulated in terms of the functions

$$X^{\pm}(k) = e^{\Gamma^{\pm}(k)}, \tag{A.7}$$

$$\Gamma^{\pm}(k) = \pm \frac{1}{2} \ln [\nu(k)] + \frac{1}{2\pi i} - \!\!\!\!\!\!\int_{-\infty}^{\infty} \frac{\ln [\nu(p)]}{p - k} dp, \tag{A.8}$$

which satisfy

$$X^{+}(k) = \nu(k) X^{-}(k). \tag{A.9}$$

The solution for F_L, F_R is then expressed as

$$F_L(k) = \frac{s(k)}{2} + \frac{X^{+}(k)}{2\pi i} - \!\!\!\!\!\!\int_{-\infty}^{\infty} \frac{s(q)}{X^{+}(q)} \frac{dq}{q - k}, \tag{A.10}$$

$$F_R(k) = -\frac{s(k)}{2\nu(k)} + \frac{X^{-}(k)}{2\pi i} - \!\!\!\!\!\!\int_{-\infty}^{\infty} \frac{s(q)}{X^{+}(q)} \frac{dq}{q - k}. \tag{A.11}$$

The inverse Fourier transform of these functions results in the current density in the regions $x < 0$ and $x > 0$, respectively, as can be seen from equations (A.1) and (A.2).

Let us examine equation (A.10) in more detail. By simple algebraic manipulations, this equation is rewritten as

$$F_L(k) = \frac{s(k)}{2} + \frac{1}{2\pi i} - \!\!\!\!\!\!\int_{-\infty}^{\infty} \frac{s(q) dq}{q - k} + \tilde{J}_x^{s,L}(k), \tag{A.12}$$

$$\tilde{J}_x^{s,L}(k) = -\frac{1}{2\pi i} \int_{-\infty}^{\infty} \frac{X^{+}(q) - X^{+}(k)}{q - k} \frac{s(q) dq}{X^{+}(q)}. \tag{A.13}$$

For $x < 0$, the inverse Fourier transform of the first two terms on the right-hand side of (A.12) yields the current density induced on a layer with the uniform conductivity σ_L. (It yields zero in the region $x > 0$.) This follows from the earlier remark about $s(k)$ and equation (3). Therefore, $\tilde{J}_x^{s,L}(k)$ is the

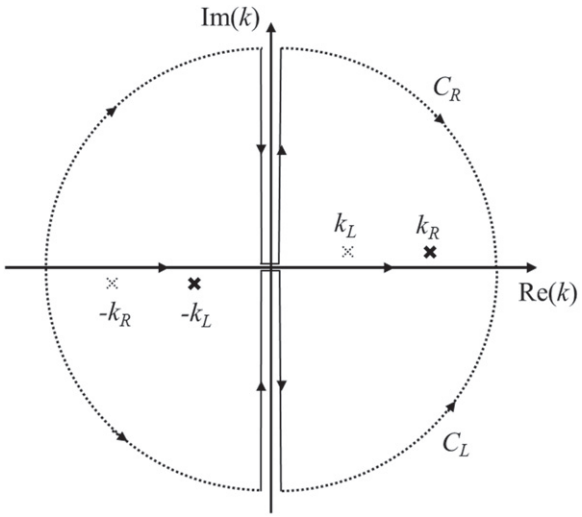

Figure A.1. Integration paths for the calculation of current density. C_L and C_R are used for $x < 0$ and $x > 0$, after taking account of the poles at $-k_L$ and k_R, respectively. The contribution of the semicircles vanishes as their radii approach infinity, leaving the branch-cut integrals along the negative and positive imaginary axes for the two cases.

Fourier transform of the scattered current density due to the discontinuity at $x = 0$. Note also that the integral in (A.13) is a conventional one since the integrand has no singularity at $k = q$.

Although the method outlined is of general applicability, we neglect the losses and take k_L, k_R to be real. (In order to ensure causality, k_L and k_R are actually assumed to possess infinitesimal, positive imaginary parts in the calculations.) A simple expression can then be found for X^+ (see appendix B),

$$X^+(k) = e^{i\Psi(k)}\left(\frac{k_L + |k|}{k_R + |k|}\right)^{1/2}\frac{k_R + k}{k_L + k}, \tag{A.14}$$

$$\Psi(k) = \frac{k}{\pi}\int_0^\infty \arctan\left[\frac{(k_L - k_R)\tau}{k_R k_L + \tau^2}\right]\frac{d\tau}{\tau^2 + k^2}. \tag{A.15}$$

When analytically continued into the complex k-plane, $X^+(k)$ has a pole at $-k_L$ and a branch cut along the negative imaginary axis, across which both $|k| = \sqrt{k^2}$ and $\Psi(k)$ are discontinuous. (Their effects cancel out across the positive imaginary axis.) On the other hand, $X^-(k)$, which is related to $X^+(k)$ by (A.9), has a pole at k_R and a branch cut along the positive imaginary axis (see figure A.1).

Let us next assume that, in the absence of the discontinuity at $x = 0$, i.e., on a graphene layer with a uniform conductivity σ_L, the external sources generate an incident current wave $J_x^i(x) = Ae^{ik_L x}$. The Fourier transform of this function is

$$s(k) = 2\pi A\delta(k - k_L), \tag{A.16}$$

which, after substitution in (A.13) gives

$$\tilde{J}_x^{s,L}(k) = \frac{iA}{X^+(k_L)}\frac{X^+(k_L) - X^+(k)}{k_L - k}. \tag{A.17}$$

The scattered current in the region $x < 0$ is found by taking the inverse Fourier transform

$$J_x^{s,L}(x) = \frac{1}{2\pi}\int_{-\infty}^{\infty}\tilde{J}_x^{s,L}(k)e^{ikx}dk, \tag{A.18}$$

which can be evaluated by deforming the path of integration into the lower half of the complex k-plane (figure A.1). Because of the presence of $X^+(k)$ in (A.17), $\tilde{J}_x^{s,L}(k)$ has a pole at $k = -k_L$ and a branch cut along the negative imaginary axis. The residue of the pole yields the reflected wave

$$J_x^r(x) = e^{2i\Psi(-k_L)}\frac{k_L - k_R}{k_L + k_R}Ae^{-ik_L x}, \tag{A.19}$$

where we have used $\Psi(k) = -\Psi(-k)$. The branch cut produces an evanescent field that decays rapidly away from the junction at $x = 0$.

To calculate the current density in the region $x > 0$, equation (A.11) is first recast into a form similar to (A.12). Using $s(k_L)/\nu(k_L) = 0$, which is a consequence of (A.4), (A.16), the Fourier transform of the current density is written as

$$\tilde{J}_x^{s,R}(k) = -F_R(k) = \frac{-iA}{X^+(k_L)}\frac{X^-(k_L) - X^-(k)}{k_L - k}. \tag{A.20}$$

This function has a pole at $k = k_R$ and a branch cut along the positive imaginary axis, both due to $X^-(k)$. After taking the inverse Fourier transform of $\tilde{J}_x^{s,R}(k)$ by deforming the path of integration into the upper half of the complex k-plane (figure A.1), the residue of the pole yields the transmitted current wave

$$J_x^t(x) = \frac{2(k_L k_R)^{1/2}}{k_L + k_R}Ae^{ik_R x}. \tag{A.21}$$

Here we have used $\Psi(k_R) = \Psi(k_L)$, which follows from (A.15) after changing the variable of integration to $1/\tau$.

Therefore, for an incident current wave $J_x^i(x) = Ae^{ik_L x}$, the scattered current well away from the discontinuity at $x = 0$ equals (A.19) for $x < 0$ and (A.21) for $x > 0$. The coefficients of reflection and transmission are given by (8). Equation (9) is obtained by noting that $\vartheta = 2\Psi(-k_L)$ and using (A.15) in which the variable of integration is changed to $\tau = k_L u$.

Appendix B. Derivation of X^+

In order to derive (A.14), (A.4) is substituted into (A.8) and the resulting principal value integral is decomposed into its real and imaginary parts, taking into account the infinitesimal,

positive imaginary parts of k_L, k_R,

$$\frac{1}{2\pi i}-\!\!\int_{-\infty}^{\infty}\ln\left(\frac{k_R-|p|}{k_L-|p|}\right)\frac{dp}{p-k} = -\frac{1}{2}-\!\!\int_{k_L}^{k_R}\frac{dp}{p-k} \quad -\frac{1}{2}-\!\!\int_{-k_R}^{-k_L}\frac{dp}{p-k} + \frac{1}{2\pi i}-\!\!\int_{-\infty}^{\infty}\ln\left|\frac{k_R-|p|}{k_L-|p|}\right|\frac{dp}{p-k}. \tag{B.1}$$

After using the pair of integrals (Hilbert transforms)

$$\frac{1}{\pi}-\!\!\int_a^b\frac{dp}{p-k}=\frac{1}{\pi}\ln\left|\frac{b-k}{a-k}\right|, \tag{B.2}$$

$$\frac{1}{\pi^2}-\!\!\int_{-\infty}^{\infty}\ln\left|\frac{b-p}{a-p}\right|\frac{dp}{p-k}=\theta(k-b)-\theta(k-a), \tag{B.3}$$

in which θ is the Heaviside step function, and combining the results, it is found that

$$\frac{1}{2\pi i}-\!\!\int_{-\infty}^{\infty}\ln\left(\frac{k_R-|p|}{k_L-|p|}\right)\frac{dp}{p-k} = i\Psi(k)+\frac{1}{2}\ln\left(\frac{k_R+k}{k_L+k}\right) -\frac{1}{2}\ln\left(\frac{k_R-k}{k_L-k}\right), \tag{B.4}$$

with

$$\Psi(k)=\frac{k}{\pi}-\!\!\int_0^{\infty}\ln\left(\frac{k_R+p}{k_L+p}\right)\frac{dp}{p^2-k^2}. \tag{B.5}$$

Substitution of (B.4) into (A.8) and (A.7), followed by simple algebraic manipulations, leads to (A.14). Equation (B.5) can be transformed into (A.15) by deforming its path of integration into the imaginary axis in the complex k-plane.

Appendix C. Power carried by graphene plasmons in the quasi-static approximation

In this appendix, we show that the power carried by a GP is proportional to the square of the surface current density amplitude, and thus the reflected and transmitted powers are $|r|^2$ and $|t|^2$, respectively. Let us assume that graphene is embeded in a medium with permittivity ϵ_e. The electromagnetic fields of the GP mode are

$$E_x=Ae^{-\alpha|z|}e^{ik_Px}, \tag{C.1}$$

$$H_y=\mathrm{sgn}(z)\frac{\omega\epsilon_e}{i\alpha}Ae^{-\alpha|z|}e^{ik_Px}, \tag{C.2}$$

$$E_z=\mathrm{sgn}(z)\frac{k_P}{i\alpha}Ae^{-\alpha|z|}e^{ik_Px}, \tag{C.3}$$

where k_P is the GP's propagation constant, $\alpha^2=k_P^2-(\omega/c)^2\epsilon_e$ and c is the speed of light in a vacuum. The time-averaged power per unit length is then obtained as

$$P=\frac{1}{2}\mathrm{Re}\left(\int_{-\infty}^{\infty}E_zH_y^*dz\right)=|A|^2\frac{\omega\epsilon_e\,\mathrm{Re}(k_P)}{2\,|\alpha|^2\,\mathrm{Re}(\alpha)}\approx|A|^2\frac{\omega\epsilon_e}{2\,|\alpha|^2}, \tag{C.4}$$

where it is assumed that $\alpha\approx k_P$ under quasi-static approximation. On the other hand, the surface current density on graphene is

$$J_x=\sigma E_x(z=0)\approx\frac{2i\omega\epsilon_e}{\alpha}Ae^{ik_Px}. \tag{C.5}$$

Therefore, from (C.5) and (C.4) and for constant ϵ_e and ω we have

$$P\propto|J_x|^2, \tag{C.6}$$

which is the sought-after relation.

References

[1] Novoselov K S, Geim A K, Morozov S V, Jiang D, Zhang Y, Dubonos S V, Grigorieva I V and Firsov A A 2004 Electric field effect in atomically thin carbon films *Science* **306** 666–9

[2] Jablan M, Buljan H and Soljačić M 2009 Plasmonics in graphene at infrared frequencies *Phys. Rev.* B **80** 245435

[3] Alaee R, Farhat M, Rockstuhl C and Lederer F 2012 A perfect absorber made of a graphene micro-ribbon metamaterial *Optics Express* **20** 28017–24

[4] Singh P, Kumar J, Toma F M, Raya J, Prato M, Fabre B, Verma S and Bianco A 2009 Synthesis and characterization of nucleobase- carbon nanotube hybrids *J. Am. Chem. Soc.* **131** 13555–62

[5] Khavasi A and Rejaei B 2014 Analytical modeling of Graphene Ribbons as optical circuit elements *IEEE J. Quantum Electron.* **50** 397–403

[6] Llatser I, Kremers C, Cabellos-Aparicio A, Jornet J M, Alarcón E and Chigrin D N 2012 Graphene-based nano-patch antenna for terahertz radiation *Photonics and Nanostructures-Fundamentals and Applications* **10** 353–8

[7] Vakil A and Engheta N 2011 Transformation optics using graphene *Science* **332** 1291–4

[8] Zhuang H-W, Kong F-M, Li K and Yue Q-Y 2014 A gating tunable planar lens based on graphene *Opt. Quantum Electron.* **47** 1139–50

[9] Forati E, Hanson G W, Yakovlev A B and Alù A 2014 Planar hyperlens based on a modulated graphene monolayer *Phys. Rev.* B **89** 081410

[10] Garcia-Pomar J L, Nikitin A Y and Martin-Moreno L 2013 Scattering of graphene plasmons by defects in the graphene sheet *ACS Nano* **7** 4988–94

[11] Nikitin A Y, Low T and Martin-Moreno L 2014 Anomalous reflection phase of graphene plasmons and its influence on resonators *Phys. Rev.* B **90** 041407

[12] Rosolen G and Maes B 2015 Nonuniform doping of graphene for plasmonic tapers *J. Opt.* **17** 015002

[13] Koppens F H L, Chang D E and Garcia de Abajo F J 2011 Graphene plasmonics: a platform for strong light-matter interactions *Nano Letters* **11** 3370–7

[14] Falkovsky L and Varlamov A 2007 Space-time dispersion of graphene conductivity *European Physics Journal* B **56** 281–4

[15] Hanson G W 2008 Dyadic Green's functions and guided surface waves for a surface conductivity model of graphene *J. Appl. Phys.* **103** 064302

[16] Muskhelishvili N I 1953 *Singular Integral Equations: Boundary Problems of Function Theory and Their Application to Mathematical Physics* (Noordhoff: Dover Publications)